AGU
ADVANCING EARTH AND SPACE SCIENCE

Geophysical Research Letters®

Key Points:
- The inter-annual variability of the CH_4 flux between the stratosphere and the troposphere is 2.0 Tg a^{-1}
- Globally the stratosphere-troposphere exchange is a minor contributor to observed inter-annual variation of tropospheric CH_4 growth
- The surface impact can be substantial at high latitudes during the maximum or minimum of the Brewer-Dobson Circulation

Correspondence to:

Y. Zhang,
zhangyuzhong@westlake.edu.cn

Author Contributions:

Conceptualization: Peixuan Zhang, Yuzhong Zhang
Formal analysis: Peixuan Zhang
Methodology: Peixuan Zhang, Ruosi Liang, Wei Chen, Xinchun Xie
Supervision: Yuzhong Zhang
Visualization: Peixuan Zhang
Writing – original draft: Peixuan Zhang
Writing – review & editing: Yuzhong Zhang

Evaluation of the Stratospheric Contribution to the Inter-Annual Variabilities of Tropospheric Methane Growth Rates

Peixuan Zhang[1,2,3], Yuzhong Zhang[2,3] , Ruosi Liang[2,3,4] , Wei Chen[2,3,4], and Xinchun Xie[2,3,4]

[1]Fudan University, Shanghai, China, [2]Key Laboratory of Coastal Environment and Resources of Zhejiang Province, School of Engineering, Westlake University, Hangzhou, China, [3]Institute of Advanced Technology, Westlake Institute for Advanced Study, Hangzhou, China, [4]Zhejiang University, Hangzhou, China

Abstract Tropospheric methane (CH_4) shows large inter-annual variability in its growth rates on top of decadal trends, which is usually interpreted as changes in sources or sinks. The contribution of the stratosphere-troposphere exchange (STE) is often omitted in such analyses. Here, we quantify annual anomalies of stratosphere-troposphere CH_4 fluxes using varied model- or observation-based methods. Globally, the inter-annual variability (standard deviation) of this flux during 2000–2020 is 2.0 Tg a^{-1}, producing a variability of ~0.6 ppb a^{-1} at the surface, which is only ~20% of observed surface CH_4 growth rate variability. Compared to global averages, high latitudes experience a larger STE-induced surface variability, which is 80% of the observed surface anomalies in the Antarctic and 44% in the Arctic. Our results suggest that although the STE process is a minor contributor globally, it has a considerable impact over polar regions on the inter-annual variability of surface CH_4 growth rates.

Plain Language Summary In addition to surface emissions and tropospheric removal, tropospheric CH_4 concentrations are also affected by exchange with the stratosphere. However, the changes in the stratosphere-troposphere flux are often unaccounted for in the analysis of surface CH_4 observations. Here we evaluate this stratospheric influence by quantifying stratosphere-troposphere CH_4 fluxes. We find that the surface CH_4 variability induced by the stratosphere-troposphere exchange is relatively small globally but can be substantial in polar regions at anomalies of the stratospheric circulation.

1. Introduction

Methane (CH_4) is the second biggest contributor to human-caused climate change after CO_2. Surface in situ measurements show that tropospheric concentrations of CH_4 have been increasing since the 1980s, followed by a period of stabilization from 2000 to 2007 (Dlugokencky et al., 2003). The increase resumed in 2007 (M. Rigby et al., 2008) with a sign of acceleration after 2014 (Nisbet et al., 2019; Zhang et al., 2021). Superimposed on these long-term changes are large inter-annual variabilities in growth rates (i.e., temporal tendency of tropospheric concentrations) (Lan et al., 2023). The drivers for long-term trends and inter-annual variabilities of CH_4 growth, however, are not well understood. For instance, studies disagree on the cause of the resumed CH_4 increase since 2007 (Hausmann et al., 2016; Matthew Rigby et al., 2017; Saunois et al., 2017; Schaefer et al., 2016; Turner et al., 2017; Worden et al., 2017) and the remarkably strong increase in 2020 (Feng et al., 2023; Peng et al., 2022; Qu et al., 2022; Schuh et al., 2019; Stevenson et al., 2022).

The tropospheric growth rate of a well-mixed gas (e.g., CH_4) reflects the imbalance of three competing processes, surface emissions, tropospheric loss, and exchange with the stratosphere:

$$\frac{dB_T}{dt} = E_T - L_T + F_{S \to T} \tag{1}$$

where E_T is surface emissions, L_T is tropospheric loss, and $F_{S \to T}$ is the stratosphere-to-troposphere flux. B_T represents the tropospheric burden and hence $\frac{dB_T}{dt}$ the growth rate of the tropospheric burden. Most analyses of surface CH_4 observations focus on variations of sources (E_T, natural or anthropogenic emissions) and sinks (L_T, oxidation by tropospheric OH), but little discussion has been made to elucidate the impact of the stratosphere-troposphere-exchange (STE) on inter-annual anomalies of CH_4 growth rates.

Previous studies have demonstrated that the $F_{S \to T}$ term has a considerable impact on the tropospheric concentrations of N_2O, another well-mixed greenhouse gas, at seasonal and inter-annual scales (Lickley et al., 2021; Nevison et al., 2004, 2011; Ray et al., 2020; Ruiz et al., 2021; Ruiz & Prather, 2022; Thompson et al., 2013). Driven by the global-scale Brewer-Dobson circulation, N_2O-rich tropospheric air enters the stratosphere (where N_2O is destroyed by photochemistry) in the tropics, and N_2O-depleted stratospheric air returns to the troposphere in the extra-tropics, leading to a net troposphere-to-stratosphere N_2O flux ($F_{S \to T} < 0$) (Ruiz et al., 2021). The variability of $F_{S \to T}$ is modulated by the Quasi-Biennial Oscillation (QBO) (Baldwin et al., 2001; Ruiz et al., 2021), that is, the westerly QBO phase is associated with a weaker circulation and subsequently a positive $F_{S \to T}$ anomaly, while the easterly QBO phase is associated with the opposite. The effect can propagate from the tropopause down to the surface with a lag of a few months, producing a periodic signal in surface observations of N_2O growth rates with a cycle of ~28-month and a relative magnitude of 0.1%–0.2% a^{-1} (Ray et al., 2020).

The same transport process should also affect CH_4 fluxes between the troposphere and the stratosphere. Meanwhile, chemical loss processes differ greatly between CH_4 and N_2O. While N_2O is primarily removed in the stratosphere (Tian et al., 2020), CH_4 is primarily destroyed in the troposphere through oxidation by the OH radical (~90% of the total sink) with a minor chemical loss in the stratosphere (Saunois et al., 2020). As a result, $F_{S \to T}$ is on average a minor term in the tropospheric CH_4 budget, compared to E_T or L_T. However, this does not necessarily rule out that the inter-annual variability of $F_{S \to T}$ can be an appreciable contributor to the inter-annual variability of $\frac{dB_T}{dt}$ for CH_4. If so, interpreting observed surface CH_4 growth without accounting for it may lead to biased attribution to the changes in CH_4 emissions or global OH concentrations. We will quantitively examine the contribution of $F_{S \to T}$ to surface CH_4 growth rate anomalies in this study.

2. Data and Methods

### 2.1. Inter-Annual Variability of Greenhouse Gas Growth Rates

We derive the inter-annual variability of atmospheric growth of N_2O and CH_4 from monthly marine boundary layer observations of their mole fractions from the National Oceanic and Atmospheric Administration (NOAA) Earth System Research Laboratories (ESRL) (Lan et al., 2023). We first compute annual growth rates by taking 1-year differences for each month from the 1-year running averaged monthly time series. To derive the inter-annual variability of growth rates, we then subtract 5-year running averages of the annual growth rates from their 1-year running averages. This operation preserves inter-annual signals on the time scales of 1–5 years and removes short-term seasonality and long-term trends (Ray et al., 2020). Figures 1a and 1b illustrate our computation of 1-year and 5-year running averages of growth rates for N_2O and CH_4. We also apply the same procedure to other simulated or derived time series in this study to obtain inter-annual variability of growth rates.

2.2. Diagnostics of Stratosphere-Troposphere CH_4 fluxes

We use three methods (i.e., fixed-budget simulation, tracer scaling, and residual circulation velocity) to estimate CH_4 fluxes between the stratosphere and troposphere ($F_{S \to T}$).

The fixed-budget simulation method is based on a chemical transport simulation of CH_4 mole fractions driven by a uniform surface CH_4 emission field (~518 Tg a^{-1}) invariant in time and space. The annually invariant monthly 3-D tropospheric OH field (a global CH_4 lifetime against tropospheric OH oxidation: ~11.0 a) is taken from a GEOS-Chem full chemistry simulation (Wecht et al., 2014) and the monthly stratospheric loss frequency field (the stratospheric CH_4 lifetime: ~35 a) from the NASA Global Modeling Initiative model (Murray et al., 2012). The resulting inter-annual variability of surface CH_4 mole fractions can then be attributed to the stratosphere-troposphere exchange. A similarly configured simulation was used by Prather (2022) to investigate the effect of STE on surface CO_2 variability. The simulation is conducted for 1996–2020 with the GEOS-Chem (12.9.3) model (CH_4-only mode) where the first 4 years are for spin-up and the remaining 20 years are used for the analysis. We check after the spin-up that the global atmospheric burden and the stratosphere-troposphere gradient are established (close to the steady state; do not increase or decrease monotonically) to ensure that the CH_4 anomaly derived from the simulation is free from artifacts caused by relaxation to the steady state. The simulation has a horizontal resolution of $4° \times 5°$ and 47 vertical layers (30 layers in the troposphere) and is driven by meteorological fields from the MERRA-2 reanalysis (Gelaro et al., 2017).

The second method is the tracer scaling method. We scale the inter-annual variability of observed surface N_2O growth rates (as derived in Section 2.1) with the observed tracer ratio of CH_4 to N_2O near the tropopause (Ruiz & Prather, 2022; Sankey & Shepherd, 2003). The mole fraction ratio between CH_4 and N_2O is determined to be 4.3,
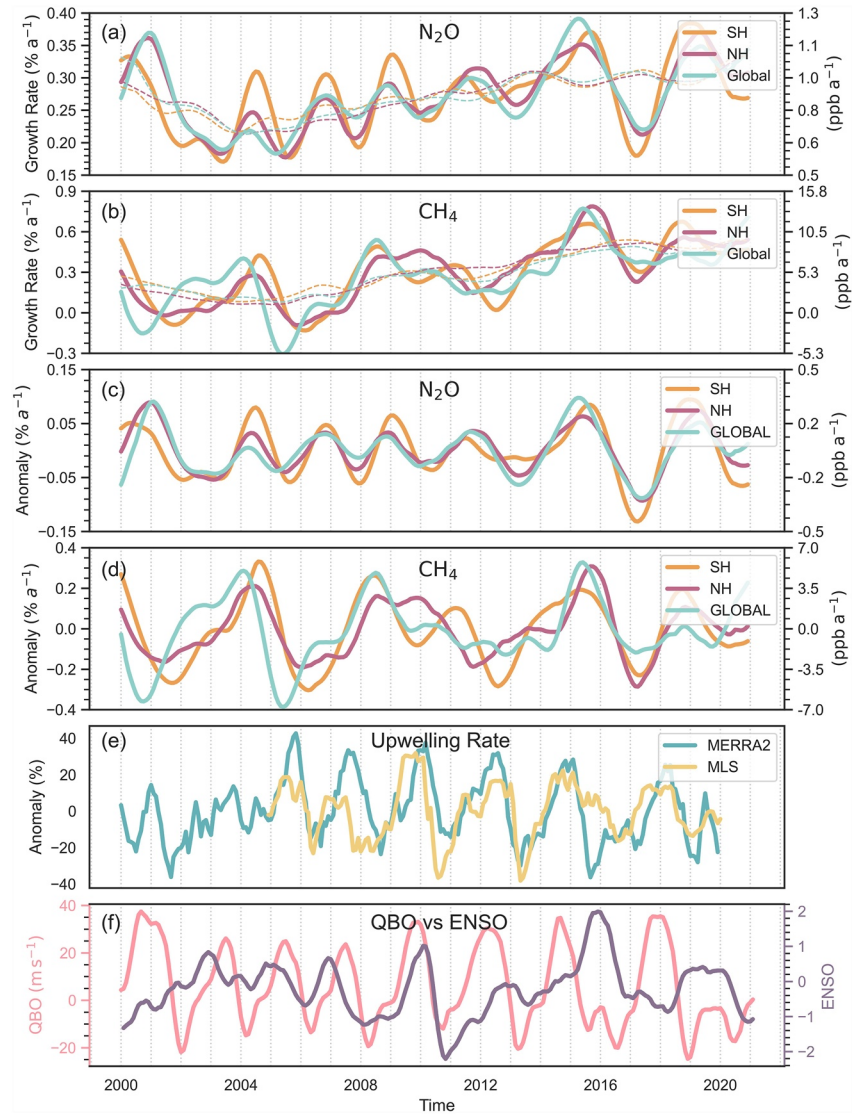
Figure 1. (a and b) Annual growth rates of surface N$_2$O and CH$_4$ mole fractions. Solid lines are 1-year running averages and dashed lines are 5-year running averages (c and d) Inter-annual variability of N$_2$O and CH$_4$ growth rates obtained by subtracting the 1-year running averages from the 5-year running averages shown in panel (a and b). (e) Time series of deseasonalized monthly tropical upwelling rate anomalies, which is derived from MERRA2 and MLS water vapor measurements (8°S–8°N) (Flury et al., 2013; Neu et al., 2014; Schoeberl et al., 2008). (f) Multivariate ENSO and shear QBO index from 2000 to 2020. Multivariate ENSO index is adopted from NOAA (https://psl.noaa.gov/enso/dashboard.html; Accessed on 20 April 2023), and the QBO index refers to the difference between 50 and 20 hPa zonal wind measured at Singapore (Neu et al., 2014).

based on the regression slope from their ACE-FTS satellite observations (Atmospheric Chemistry Experiment –Fourier Transform Spectrometer, level 2 version 4.1 (Bernath, 2017)) in the lower stratosphere (Figure S1). A similar slope is also found in the GEOS-Chem simulation (Figure S1). The premise of the N$_2$O-scaling method is that the stratosphere-troposphere-exchange is the dominant process controlling the inter-annual variability of surface N$_2$O concentrations (Nevison et al., 2004; Ruiz et al., 2021).

The third method is to calculate stratosphere-troposphere CH$_4$ fluxes with the transformed Eulerian mean vertical velocity ($\overline{w^*}$) based on the transformed Eulerian mean formulation (Equation 2) (Hoppe et al., 2016; Remsberg, 2015):

$$\overline{w^*} = \overline{w} + (a\cos\varphi)^{-1}\left(\frac{\cos\varphi\overline{v'\theta'}}{\overline{\theta_z}}\right)_\varphi \tag{2}$$
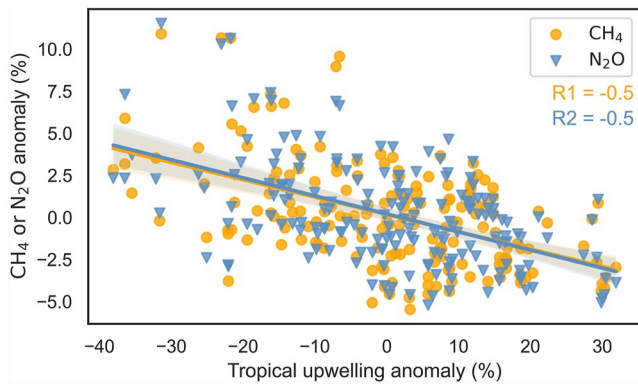
Figure 2. Relationships between tracer (CH_4 or N_2O) abundance anomalies observed by ACE-FTS in the lowermost stratosphere (150 hPa) between 40°N and 50°N and tropical upwelling anomalies derived from MLS water vapor observations. Tropical upwelling anomalies lead tracer abundance anomalies by 5 months. Correlation coefficients are inset.

where $\overline{w}$ represents the mean vertical velocity and $\overline{v'\theta'}$ is the meridional eddy heat flux (overbar denotes zonal mean). $\overline{w}$ and $\overline{v'\theta'}$ are computed from 3-hourly MERRA-2 reanalyzed meteorological fields. Additionally, a represents the radius of the Earth, z altitude, and φ latitude. The subscripts z and φ represent partial derivatives with respect to altitude and latitude respectively. We integrate globally advective CH_4 flux densities that are computed as the product of the vertical residual velocity ($\overline{w^*}$; m s^{-1}) and observed CH_4 concentrations ($\overline{CH_4}$; g m^{-3}) near the tropopause. The computation is conducted on a monthly basis. Near-tropopause CH_4 concentrations are derived from ACE-FTS observations.

3. Results

3.1. Inter-Annual Variability of Atmospheric Growth Rates of CH_4 and N_2O

Figures 1c and 1d show the inter-annual anomalies of tropospheric CH_4 and N_2O growth rates during 2000–2020, after removing short-term seasonality and long-term trends. The inter-annual anomalies of tropospheric N_2O growth rates show a pronounced cycle with a period of about 28 months and an amplitude of around ±0.1% (standard deviation), and are in phase with the Brewer-Dobson Circulation variability (expressed as tropical upwelling velocity anomalies) (Figure 1e) and the QBO (Figure 1f). The deseasonalized zonal mean tropical upwelling velocities in Figure 1e are derived from either meteorological data (MERRA-2) or satellite water vapor measurements (MLS). For the latter, upwelling velocities are derived from the ascent time of satellite-observed water vapor between two pressure levels in the lower-to mid-stratosphere for 8°S–8°N (Flury et al., 2013; Neu et al., 2014; Schoeberl et al., 2008). The QBO shear index in Figure 1f is computed as the difference of the zonal wind between 50 hPa and 20 hPa in Singapore (Neu et al., 2014). Our result is consistent with previous findings that the inter-annual variability in surface N_2O is dominated by the net flux of N_2O between the stratosphere and the troposphere (Nevison et al., 2004, 2011; Ruiz et al., 2021). The two hemispheres are well in sync, also indicating that a global-scale process is at play, as it takes time for regional signals to propagate to the globe.

In comparison, the inter-annual anomalies of the tropospheric CH_4 growth rate (Figure 1c) have a relative magnitude of ±0.3% (standard deviation), which is larger than that of N_2O (±0.1%). The periodicity is also less pronounced for CH_4 compared to the 28-month cycle for N_2O (Figures 1c and 1d). The growth rate anomalies of CH_4 do not in general correspond to that of N_2O, the Brewer-Dobson Circulation strength, and the QBO (Figures 1c–1e), implying that the variability of surface CH_4, unlike that of N_2O, is not controlled by the stratospheric influence ($F_{S \to T}$). This is not unexpected as studies have shown substantial inter-annual variabilities of both tropospheric CH_4 sources and sinks (Bloom et al., 2017; Montzka et al., 2011). The above analyses, however, do not rule out the stratosphere-troposphere exchange as a potential contributor to the inter-annual variability of tropospheric CH_4 growth. Quantification of the stratosphere-troposphere flux is required to determine to what degree surface growth rate anomalies are affected by the stratospheric influence.

In contrast to the surface analyses shown above, Figure 2 shows that both CH_4 and N_2O anomalies near the mid-latitude lower stratosphere (40°N–50°N, 150 hPa) measured by ACE-FTS are anti-correlated with the Brewer-Dobson Circulation variability (Figure 1e) with a time lag of 5 months ($R = -0.50$), implying that $F_{S \to T}$ for N_2O and CH_4 are similarly affected by the stratospheric circulation. A strengthened (weakened) stratospheric circulation, often associated with El Niño (La Niña) and easterly (westerly) shear of the QBO (Domeisen et al., 2019), enhances (suppresses) downward transport of CH_4- and N_2O-depleted air from the higher part of the stratosphere (where chemical loss is strong), leading to negative (positive) anomalies in CH_4 and N_2O abundance near the mid-latitude tropopause as well as in their fluxes into the troposphere.

3.2. Quantify the Contribution of Stratosphere-Troposphere Exchange to Surface CH_4 Variability

Figure 3 shows STE-induced inter-annual anomalies of CH_4 growth rates derived from the three methods described in Section 2.2. The fixed-budget simulation, N_2O-scaling, and residual circulation methods
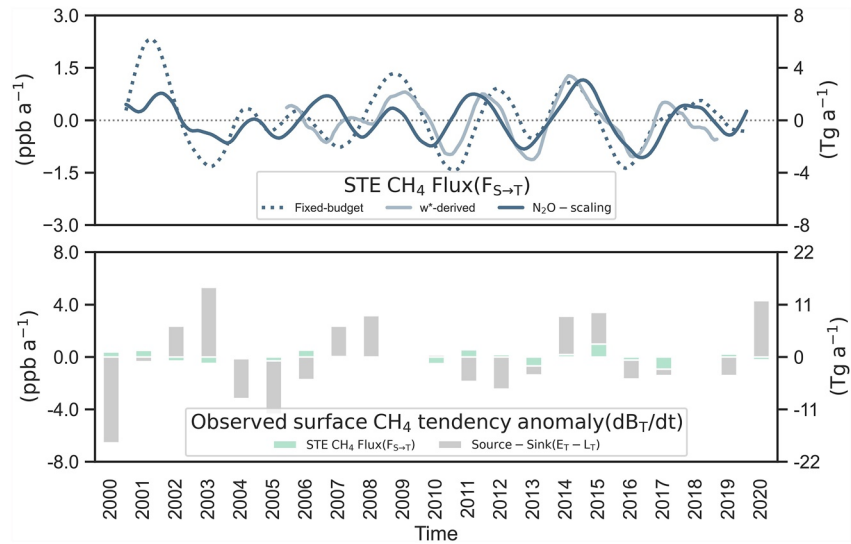
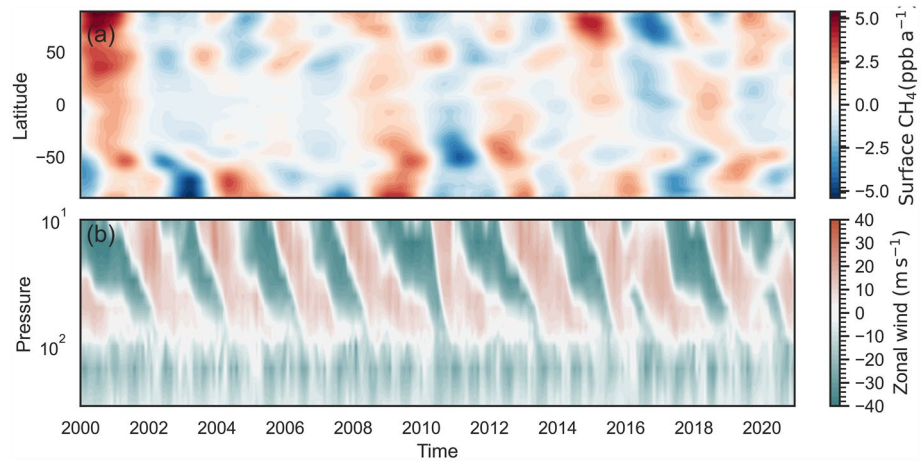**Figure 3.** (top) Surface CH_4 grow rate anomalies due to the stratosphere-troposphere flux (STE CH_4 flux) derived from different methods (N_2O-scaling, fixed-budget simulation, and w^*-method). (bottom) Comparison with observed surface CH_4 grow rate anomalies ($\frac{dB_T}{dt}$). Anomalies are expressed in ppb a^{-1} (left axis) and Tg a^{-1} (right axis).

generally achieve consistent results in both the magnitude and the phase with moderate correlation coefficients ($R_{\text{fix-budget},N_2O-\text{scaling}} = 0.50$, $R_{\text{fix-budget,residual circulation}} = 0.75$, $R_{\text{residual circulation},N_2O-\text{scaling}} = 0.54$). The inter-annual variability of the CH_4 flux between the stratosphere and the troposphere (standard deviation of time series in Figure 3a) is about 2.0 Tg a^{-1} (average of ~2.3 Tg a^{-1} for the fixed-budget method, ~1.4 Tg a^{-1} for the N_2O-scaling method, and ~1.7 Tg a^{-1} for the residual circulation method), which creates ~0.6 ppb a^{-1} anomalies at the surface. In comparison, the observed anomaly of the CH_4 annual growth rates is ~2.8 ppb a^{-1} (~7.7 Tg a^{-1}) (Figure 1d), the inter-annual variability of wetland CH_4 emissions is ~8.0 ppb a^{-1} (~20 Tg a^{-1}) based on the ensemble average of WetCHARTs bottom-up estimation (Bloom et al., 2017) and that of CH_4 removal by the OH radical is ~3.6 ppb a^{-1} (~10 Tg a^{-1}) based on 5% inter-annual changes in the global OH concentration reported in the literature (Montzka et al., 2011). Given the dominance of surface emission (E_T) and tropospheric oxidation (L_T), the STE signal ($F_{S \to T}$) is unlikely to be discerned from surface observations of CH_4 when integrated over the troposphere, which contrasts with N_2O. Further inspection of Figure 3 shows that $F_{S \to T}$ is also a minor player in individual years when strong positive (e.g., 2003, 2014, 2015, and 2020) and negative (e.g., 2000 and 2005) methane growth rate anomalies are observed at the surface.

Given the small magnitude of $F_{S \to T}$ variations, the moderate correlation between $F_{S \to T}$ and $\frac{dB_T}{dt}$ ($R = 0.43$) (Figure 3) also suggests some covariations of $F_{S \to T}$ with E_T and/or L_T, indicating that they are regulated by common factors, such as ENSO and QBO. For instance, ENSO modulates variabilities in wetland methane emissions (Zhu et al., 2017) and in tropospheric oxidation (Rowlinson et al., 2019; Turner et al., 2018). QBO can modulate the tropospheric oxidation of CH_4 through its effects on stratospheric ozone and subsequently downward ultraviolet flux (Hamilton & Fan, 2000). Our results also show that the correlation is stronger with CH_4 growth rates in the Southern Hemisphere than those in the Northern Hemisphere ($R_{NH} = 0.33$; $R_{SH} = 0.53$) and is stronger in 2010–2020 than 2000–2010 ($R_{2000-2010} = 0.18$, $R_{2010-2020} = 0.55$).

Figure 4a shows surface CH_4 growth rates derived from the fixed-budget simulation as a function of latitude and time. Although the STE-induced surface anomalies occur roughly simultaneously across all latitudes, the magnitude of the surface impacts is not spatially uniform. The largest effect often occurs at high latitudes where the Brewer-Dobson Circulation drives the downward transport of stratospheric air. Based on the fixed-budget simulation, the STE process is responsible for the inter-annual variability (standard deviation) of 1.76 ppb a^{-1} in the Antarctic and 1.79 ppb a^{-1} in the Arctic, which are respectively 80% and 43% of the CH_4 growth rate variability observed at the Antarctic (2.22 ppb a^{-1}; average of two sites in 70°S–90°S; Halley Station and South Pole) and the Arctic surface sites (4.13 ppb a^{-1}; average of six sites in 70°N–90°N; Alert, Barrow, Mould Bay, Summit, Hydrometeorological Observatory of Tiksi, and Ny-Alesund) (Figure 5). In comparison, the STE-induced surface
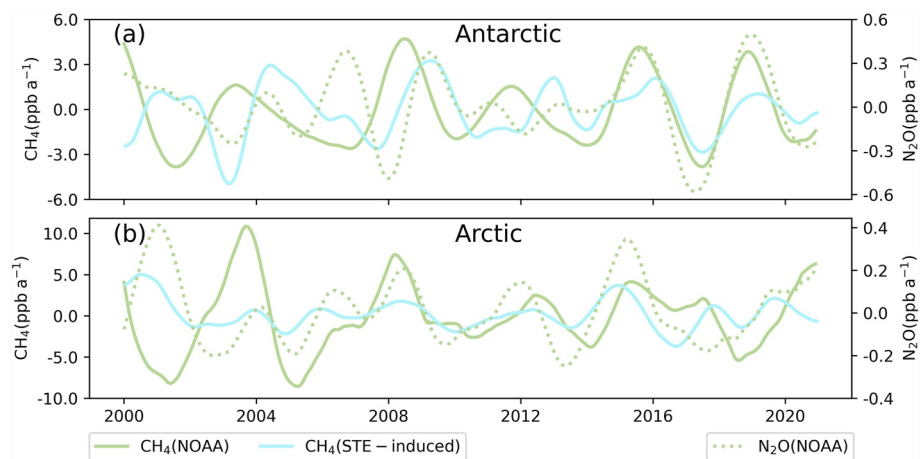
Figure 4. (a) Surface CH_4 growth rate anomalies (ppb a^{-1}) derived from the fixed-budget simulation, as a function of time and latitude. (b) Monthly mean zonal wind (m s^{-1}) derived from Singapore radiosondes (1°N, 104°E) between 70 and 10 hPa. Positive values represent westerlies.

anomalies are only 20% of observed anomalies globally (Figure 3). The stratospheric influence is also supported by concurrent anomalies in N_2O observations at these high-altitude surface sites (Figure 5). These results indicate that the STE-induced CH_4 flux is an important factor, in addition to tropospheric sources and sinks, for interpreting high-latitude surface observations.

Figure 4a also shows cases of extreme STE-induced surface growth rate anomalies, for example, 2000–2001 and 2015–2017 in the Arctic and 2003–2004 in the Antarctic. The physical mechanisms leading to these enhanced anomalies are yet unclear. We note that the 2015–2017 event corresponds to an anomalous QBO during which the westerly phase in 2015/2016 is extended into mid-2018, instead of shifting to the easterly phase in 2016/2017 (Figure 4b) (Kang et al., 2022).

4. Conclusions

This work analyzes the contribution of the stratosphere-troposphere exchange (STE) to the inter-annual anomalies of tropospheric CH_4 growth rates.

Figure 5. Surface growth rate anomalies of N_2O and CH_4 during 2000–2020 at (a) the Antarctic (70°S-90°S) and (b) the Arctic (70°N–90°N) NOAA surface sites. The STE-induced CH_4 growth rate anomalies are derived from the fixed-budget simulation.

We examine the inter-annual growth rate anomalies of CH_4 derived from global surface observations. We find that it is at most weakly correlated with the Brewer-Dobson Circulation and the QBO indices that characterize the variations in the STE. In contrast, the inter-annual growth rate anomalies of N_2O, which has shown in previous studies to be controlled by the STE (Lickley et al., 2021; Nevison et al., 2004, 2011; Ray et al., 2020), have significant correlations with these indices. This result is consistent with the fact that the tropospheric sources and sinks play an important role for CH_4, compared to N_2O, but does not indicate that the contribution of the stratosphere-troposphere CH_4 flux is negligible in all cases.

We then quantify the impact of STE on tropospheric CH_4 concentrations, using three methods (i.e., the fixed-budget simulation method, the N_2O-scaling method, and the residual circulation velocity or w^* method). These methods, though based on varied principles and techniques, all achieve consistent CH_4 STE-induced fluxes for 2000–2020. The results show that the standard deviation of the STE-induced CH_4 flux is 2.0 Tg a^{-1}, equivalent to a 0.6 ppb a^{-1} surface growth rate anomaly. This value is only 20% of the observed CH_4 inter-annual growth rate anomaly (2.8 ppb a^{-1}), suggesting that the STE is a minor contributor to CH_4 inter-annual growth rate anomaly on a global scale.

We further use the results from the fixed-budget simulation to show the spatial-temporal distribution of the STE-induced growth rate anomalies at the surface. We find that the STE causes surface CH_4 anomalies across all latitudes but with the largest impact at high latitudes. The inter-annual variabilities of STE-induced surface CH_4 growth rates are 80% and 44% of those observed at the Antarctic and the Arctic surface sites, respectively. The STE-induced surface anomalies are particularly large in 2000–2001 and 2015–2017 in the Arctic and 2003–2004 in the Antarctic. For example, the simulation shows that the STE causes a positive anomaly of ∼4.0 ppb a^{-1} during 2015–2016 and a negative anomaly of ∼ −4.0 ppb a^{-1} during 2016–2017 in the polar region. This signal is significant and is clearly seen in surface observations at the Arctic sites.

Our study suggests that the STE can have considerable impacts on high-latitude observations, although its impacts are minor globally. Omitting the stratospheric influence may cause misinterpretation of surface observations in Arctic or Antarctic regions, especially when the STE is at its maximum or minimum.

Data Availability Statement

We used long-term measurements of CH_4 and N_2O from the NOAA GML surface network (https://gml.noaa.gov/aftp/data/greenhouse_gases/; Accessed on 20 April 2023) (Lan et al., 2022a, 2022b). The ACE-FTS Level 2 data (level 2 version 4.1) used in this study can be obtained via: http://www.ace.uwaterloo.ca/data.php. The source code of GEOS-Chem (version 12.9.3) is freely available through https://doi.org/10.5281/zenodo.3974569. The OH and emission fields used in the fixed-budget simulation are archived at (https://www.zenodo.org/record/7847739#.ZECWdLpByUk).

References

Baldwin, M. P., Gray, L. J., Dunkerton, T. J., Hamilton, K., Haynes, P. H., Holton, J. R., et al. (2001). The quasi-biennial oscillation. *Reviews of Geophysics*, 39(2), 179–229. https://doi.org/10.1029/1999rg000073

Bernath, P. F. (2017). The atmospheric chemistry experiment (ACE). *Journal of Quantitative Spectroscopy and Radiative Transfer*, 186, 3–16. https://doi.org/10.1016/j.jqsrt.2016.04.006

Bloom, A. A., Bowman, W. K., Lee, M., Turner, J. A., Schroeder, R., Worden, R. J., et al. (2017). A global wetland methane emissions and uncertainty dataset for atmospheric chemical transport models (WetCHARTs version 1.0). *Geoscientific Model Development*, 10(6), 2141–2156. https://doi.org/10.5194/gmd-10-2141-2017

Dlugokencky, E. J., Houweling, S., Bruhwiler, L., Masarie, K. A., Lang, P. M., Miller, J. B., & Tans, P. P. (2003). Atmospheric methane levels off: Temporary pause or a new steady-state? *Geophysical Research Letters*, 30(19), 3–6. https://doi.org/10.1029/2003GL018126

Domeisen, D. I. V., Garfinkel, C. I., & Butler, A. H. (2019). The teleconnection of El Niño Southern Oscillation to the stratosphere. *Reviews of Geophysics*, 57(1), 5–47. https://doi.org/10.1029/2018RG000596

Feng, L., Palmer, P. I., Parker, R. J., Lunt, M. F., & Bösch, H. (2023). Methane emissions are predominantly responsible for record-breaking atmospheric methane growth rates in 2020 and 2021. *Atmospheric Chemistry and Physics*, 23(8), 4863–4880. https://doi.org/10.5194/acp-23-4863-2023

Flury, T., Wu, D. L., & Read, W. G. (2013). Variability in the speed of the Brewer-Dobson circulation as observed by Aura/MLS. *Atmospheric Chemistry and Physics*, 13(9), 4563–4575. https://doi.org/10.5194/acp-13-4563-2013

Gelaro, R., McCarty, W., Suárez, M. J., Todling, R., Molod, A., Takacs, L., et al. (2017). The modern-era retrospective analysis for research and applications, version 2 (MERRA-2). *Journal of Climate*, 30(14), 5419–5454. https://doi.org/10.1175/JCLI-D-16-0758.1

Hamilton, K., & Fan, S. (2000). Effects of the stratospheric quasi-biennial oscillation on long-lived greenhouse gases in the troposphere. *Journal of Geophysical Research*, 105(D16), 20581–20587. https://doi.org/10.1029/2000jd900331

Hausmann, P., Sussmann, R., & Smale, D. (2016). Contribution of oil and natural gas production to renewed increase in atmospheric methane (2007-2014): Top-down estimate from ethane and methane column observations. *Atmospheric Chemistry and Physics*, *16*(5), 3227–3244. https://doi.org/10.5194/acp-16-3227-2016

Hoppe, C. M., Ploeger, F., Konopka, P., & Müller, R. (2016). Kinematic and diabatic vertical velocity climatologies from a chemistry climate model. *Atmospheric Chemistry and Physics*, *16*(10), 6223–6239. https://doi.org/10.5194/acp-16-6223-2016

Kang, M. J., Chun, H. Y., Son, S. W., Garcia, R. R., An, S. I., & Park, S. H. (2022). Role of tropical lower stratosphere winds in quasi-biennial oscillation disruptions. *Science Advances*, *8*(27), 1–10. https://doi.org/10.1126/sciadv.abm7229

Lan, X., Dlugokencky, E. J., Mund, J. W., Crotwell, A. M., Crotwell, M. J., Moglia, E., et al. (2022a). Atmospheric methane dry air mole fractions from the NOAA GML carbon cycle cooperative global air sampling network. Version: 2022-11-21. https://doi.org/10.15138/VNCZ-M766

Lan, X., Dlugokencky, E. J., Mund, J. W., Crotwell, A. M., Crotwell, M. J., Moglia, E., et al. (2022b). Atmospheric nitrous oxide dry air mole fractions from the NOAA GML carbon cycle cooperative global air sampling network (pp. 1997–2021). Version: 2022-11-21. https://doi.org/10.15138/53g1-x417

Lan, X., Thoning, K. W., & Dlugokencky, E. J. (2023). Trends in globally-averaged CH_4, N_2O, and SF_6 determined from NOAA global monitoring laboratory measurements. Version 2023-04. https://doi.org/10.15138/P8XG-AA10

Lickley, M., Solomon, S., Kinnison, D., Krummel, P., Mühle, J., O'Doherty, S., et al. (2021). Quantifying the imprints of stratospheric contributions to interhemispheric differences in tropospheric CFC-11, CFC-12, and N_2O abundances. *Geophysical Research Letters*, *48*(15), 1–9. https://doi.org/10.1029/2021GL093700

Montzka, S. A., Krol, M., Dlugokencky, E., Hall, B., Jo, P., & Lelieveld, J. (2011). Small interannual variability of global atmospheric hydroxyl. *Science*, *331*(6013), 67–69. https://doi.org/10.1126/science.1197640

Murray, L. T., Jacob, D. J., Logan, J. A., Hudman, R. C., & Koshak, W. J. (2012). Optimized regional and interannual variability of lightning in a global chemical transport model constrained by LIS/OTD satellite data. *Journal of Geophysical Research*, *117*(20), 1–14. https://doi.org/10.1029/2012JD017934

Neu, J. L., Flury, T., Manney, G. L., Santee, M. L., Livesey, N. J., & Worden, J. (2014). Tropospheric ozone variations governed by changes in stratospheric circulation. *Nature Geoscience*, *7*(5), 340–344. https://doi.org/10.1038/ngeo2138

Nevison, C. D., Dlugokencky, E., Dutton, G., Elkins, J. W., Fraser, P., Hall, B., et al. (2011). Exploring causes of interannual variability in the seasonal cycles of tropospheric nitrous oxide. *Atmospheric Chemistry and Physics*, *11*(8), 3713–3730. https://doi.org/10.5194/acp-11-3713-2011

Nevison, C. D., Kinnison, D. E., & Weiss, R. F. (2004). Stratospheric influences on the tropospheric seasonal cycles of nitrous oxide and chlorofluorocarbons. *Geophysical Research Letters*, *31*(20), 1–5. https://doi.org/10.1029/2004GL020398

Nisbet, E. G., Manning, M. R., Dlugokencky, E. J., Fisher, R. E., Lowry, D., Michel, S. E., et al. (2019). Very strong atmospheric methane growth in the 4 Years 2014–2017: Implications for the Paris Agreement. *Global Biogeochemical Cycles*, *33*(3), 318–342. https://doi.org/10.1029/2018GB006009

Peng, S., Lin, X., Thompson, R. L., Xi, Y., Liu, G., Hauglustaine, D., et al. (2022). Wetland emission and atmospheric sink changes explain methane growth in 2020. *Nature*, *612*(7940), 477–482. https://doi.org/10.1038/s41586-022-05447-w

Prather, M. J. (2022). CO_2 surface variability: From the stratosphere or not? *Earth System Dynamics*, *13*, 703–709. https://doi.org/10.5194/esd-13-703-2022

Qu, Z., Jacob, D. J., Zhang, Y., Shen, L., Varon, D. J., Lu, X., et al. (2022). Attribution of the 2020 surge in atmospheric methane by inverse analysis of GOSAT observations. *Environmental Research Letters*, *17*(9), 094003. https://doi.org/10.1088/1748-9326/ac8754

Ray, E. A., Portmann, R. W., Yu, P., Daniel, J., Montzka, S. A., Dutton, G. S., et al. (2020). The influence of the stratospheric Quasi-Biennial Oscillation on trace gas levels at the Earth's surface. *Nature Geoscience*, *13*(1), 22–27. https://doi.org/10.1038/s41561-019-0507-3

Remsberg, E. E. (2015). Methane as a diagnostic tracer of changes in the Brewer-Dobson circulation of the stratosphere. *Atmospheric Chemistry and Physics*, *15*(7), 3739–3754. https://doi.org/10.5194/acp-15-3739-2015

Rigby, M., Montzka, S. A., Prinn, R. G., White, J. W. C., Young, D., O'Doherty, S., et al. (2017). Role of atmospheric oxidation in recent methane growth. *Proceedings of the National Academy of Sciences of the United States of America*, *114*(21), 5373–5377. https://doi.org/10.1073/pnas.1616426114

Rigby, M., Prinn, R. G., Fraser, P. J., Simmonds, P. G., Langenfelds, R. L., Huang, J., et al. (2008). Renewed growth of atmospheric methane. *Geophysical Research Letters*, *35*(22), 2–7. https://doi.org/10.1029/2008GL036037

Rowlinson, M. J., Rap, A., Arnold, S. R., Pope, R. J., Chipperfield, M. P., Mcnorton, J., et al. (2019). Impact of El Niño-Southern Oscillation on the interannual variability of methane and tropospheric ozone. *Atmospheric Chemistry and Physics*, *19*(13), 8669–8686. https://doi.org/10.5194/acp-19-8669-2019

Ruiz, D. J., & Prather, M. J. (2022). From the middle stratosphere to the surface, using nitrous oxide to constrain the stratosphere-troposphere exchange of ozone. *Atmospheric Chemistry and Physics*, *22*(3), 2079–2093. https://doi.org/10.5194/acp-22-2079-2022

Ruiz, D. J., Prather, M. J., Strahan, S. E., Thompson, R. L., Froidevaux, L., & Steenrod, S. D. (2021). How atmospheric chemistry and transport drive surface variability of N_2O and CFC-11. *Journal of Geophysical Research: Atmospheres*, *126*(8), 1–16. https://doi.org/10.1029/2020JD033979

Sankey, D., & Shepherd, T. G. (2003). Correlations of long-lived chemical species in a middle atmosphere general circulation model. *Journal of Geophysical Research*, *108*(16), 1–18. https://doi.org/10.1029/2002jd002799

Saunois, M., Bousquet, P., Poulter, B., Peregon, A., Ciais, P., Canadell, J. G., et al. (2017). Variability and quasi-decadal changes in the methane budget over the period 2000-2012. *Atmospheric Chemistry and Physics*, *17*(18), 11135–11161. https://doi.org/10.5194/acp-17-11135-2017

Saunois, M., Stavert, R. A., Poulter, B., Bousquet, P., Canadell, J. G., Jackson, R. B., et al. (2020). The global methane budget 2000-2017. *Earth System Science Data*, *12*(3), 1561–1623. https://doi.org/10.5194/essd-12-1561-2020

Schaefer, H., Fletcher, S. E. M., Veidt, C., Lassey, K. R., Brailsford, G. W., Bromley, T. M., et al. (2016). A 21st-century shift from fossil-fuel to biogenic methane emissions indicated by 13CH4. *Science*, *352*(6281), 80–84. https://doi.org/10.1126/science.aad2705

Schoeberl, M. R., Douglass, A. R., Stolarski, R. S., Pawson, S., Strahan, S. E., & Read, W. (2008). Comparison of lower stratospheric tropical mean vertical velocities. *Journal of Geophysical Research*, *113*(24), 1–11. https://doi.org/10.1029/2008JD010221

Schuh, A. E., Jacobson, A. R., Basu, S., Weir, B., Baker, D., Bowman, K., et al. (2019). Quantifying the impact of atmospheric transport uncertainty on CO_2 surface flux estimates. *Global Biogeochemical Cycles*, *33*(4), 484–500. https://doi.org/10.1029/2018GB006086

Stevenson, D. S., Derwent, R. G., Wild, O., & Collins, W. J. (2022). COVID-19 lockdown emission reductions have the potential to explain over half of the coincident increase in global atmospheric methane. *Atmospheric Chemistry and Physics*, *22*(21), 14243–14252. https://doi.org/10.5194/acp-22-14243-2022

Thompson, R. L., Dlugokencky, E., Chevallier, F., Ciais, P., Dutton, G., Elkins, J. W., et al. (2013). Interannual variability in tropospheric nitrous oxide. *Geophysical Research Letters*, *40*(16), 4426–4431. https://doi.org/10.1002/grl.50721

Tian, H., Xu, R., Canadell, J. G., Thompson, R. L., Winiwarter, W., Suntharalingam, P., et al. (2020). A comprehensive quantification of global nitrous oxide sources and sinks. *Nature*, *586*(7828), 248–256. https://doi.org/10.1038/s41586-020-2780-0

Turner, A. J., Frankenberg, C., Wennberg, P. O., & Jacob, D. J. (2017). Ambiguity in the causes for decadal trends in atmospheric methane and hydroxyl. *Proceedings of the National Academy of Sciences of the United States of America*, *114*(21), 5367–5372. https://doi.org/10.1073/pnas.1616020114

Turner, A. J., Fung, I., Naik, V., Horowitz, L. W., & Cohen, R. C. (2018). Modulation of hydroxyl variability by ENSO in the absence of external forcing. *Proceedings of the National Academy of Sciences of the United States of America*, *115*(36), 8931–8936. https://doi.org/10.1073/pnas.1807532115

Wecht, K. J., Jacob, J. D., Frankenberg, C., Jiang, Z., & Blake, R. D. (2014). Mapping of North American methane emissions with high spatial resolution by inversion of SCIAMACHY satellite data. *Journal of Geophysical Research: Atmospheric Research*, *119*(12), 7741–7756. https://doi.org/10.1002/2014JD021551.Received

Worden, J. R., Bloom, A. A., Pandey, S., Jiang, Z., Worden, H. M., Walker, T. W., et al. (2017). Reduced biomass burning emissions reconcile conflicting estimates of the post-2006 atmospheric methane budget. *Nature Communications*, *8*(1), 1–11. https://doi.org/10.1038/s41467-017-02246-0

Zhang, Y. J., Jacob, D., Lu, X. D., Maasakkers, J. R., Scarpelli, T., Sheng, J. X., et al. (2021). Attribution of the accelerating increase in atmospheric methane during 2010-2018 by inverse analysis of GOSAT observations. *Atmospheric Chemistry and Physics*, *21*(5), 3643–3666. https://doi.org/10.5194/acp-21-3643-2021

Zhu, Q., Peng, C., Ciais, P., Jiang, H., Liu, J., Bousquet, P., et al. (2017). Interannual variation in methane emissions from tropical wetlands triggered by repeated El Niño Southern Oscillation. *Global Change Biology*, *23*(11), 4706–4716. https://doi.org/10.1111/gcb.13726